PCCP

Accepted Manuscript

ROYAL SOCIETY OF CHEMISTRY

www.rsc.org/pccp

H_2O-CH_4 and H_2S-CH_4 complexes: a direct comparison through molecular beam experiments and ab-initio calculations.

David Cappelletti[1],* Alessio Bartocci[1], Federica Frati[1], Luiz F. Roncaratti[2], Leonardo Belpassi[3], Francesco Tarantelli[1], P. Aiswaryalakshmi[4,5], Elangannan Arunan[4], and Fernando Pirani[1]

[1]*Dipartimento di Chimica, Biologia e Biotecnologie, Università di Perugia, 06123, Italy*

[2] *Dipartimento di Chimica, Biologia e Biotecnologie, Università di Perugia, 06123, Italy*

[3]*Istituto di Scienze e Tecnologie Molecolari del CNR, Perugia, 06123, Italy*

[4]*Indian Institute of Science, Dept Inorgan & Phys Chem Bangalore 560012, Karnataka, India and*

[5]*Current address: Department of Chemistry, Imperial College of Science, Technology and Medicine London, UK*

(Dated: Last revision: September 15, 2015)

Abstract

New molecular beam scattering experiments have been performed to measure the total (elastic plus inelastic) cross sections as a function of the velocity in collisions between water and hydrogen sulfide projectile molecules and methane target. Measured data have been exploited to characterize range and strength of the intermolecular interaction in such systems, which are of relevance since driving the gas phase molecular dynamics and the clathrate formation. Complementary information have been obtained by rotational spectra, recorded for the hydrogen sulfide-methane complex, with a pulsed nozzle Fourier Transform Microwave Spectrometer. Extensive ab initio calculations have been performed to rationalize all the experimental findings. The combination of experimental and theoretical information established the ground for the understanding of the nature of the interaction and allows to model its basic components, including charge transfer, in these weakly bound systems. The intermolecular potential for H_2S-CH_4 is significantly less anisotropic than that for H_2O-CH_4, though both of them have potential minima that can be characterized as 'hydrogen bonded'.

INTRODUCTION

The study of strength and range of the intermolecular interaction in weakly bond aggregates or complexes, depending on the critical balance of chemical and physical contributions, represents an important objective for the investigations of the static (equilibrium) and dynamic (non equilibrium) properties of matter, in gas and condensed phase [1]. The main target is the understanding and the modeling of the weak intermolecular forces, as those promoting the formation of the hydrogen bond [2, 3]. Experiments and theoretical calculations usually are performed on simple prototypical systems, in order to propose and test models extensible to complexes of increasing complexity and larger applied interest.

The characterization of the interaction between molecules containing hydrogen atoms and other chemical species covers, from a fundamental point of view, an important role regarding the assessment of the relative contribution of the various interaction components, and is also crucial for more tangible practical interests, as applications in the crystal engineering field and in biochemistry [4–7]. In particular, intermolecular interactions of H_2O and H_2S have attracted significant interest as the former was considered a prototype for 'directional' hydrogen bonding and the later was assumed to have 'isotropic' van der Waals interaction. The recent advances in experimental and theoretical techniques have helped scientists explore very small scale 'anisotropy' and also minute 'charge transfer' leading to 'covalency and intermolcular bonding' in interactions between virtually any two atoms or molecules, including inert gases such as argon [8–10], neon and even the lightest helium [11, 12].

Molecules, such as water, ammonia, and hydrogen sulfide attract considerable attention in the context of several elementary processes even occurring in galaxies, interstellar clouds and in hydrogen-rich atmospheres of heavy planets [13–15]. Therefore the possibility of formation of weak intermolecular bonds proposes fundamental questions not only concerning their stability, but also their role on the dynamics of gas phase energy transfer phenomena. Moreover, now days, the study of systems formed by water and small nearly spherical molecules, like methane and hydrogen, is assuming remarkable importance due to the presence of deposits of clathrates hydrates [4, 5, 16, 17], non-stochiometric compounds formed by water cages and small guest gas molecules.

A full description of the nature of weak interactions requires a quantitative knowledge of the balancing of their basic components, as the electrostatic, dispersion, induction, and size

repulsion contributions. A special focus is on the role of the charge transfer (of chemical nature) in stabilizing intermolecular bonds, which is challenging to separate from other effects [9]. Presently, it is well known that the ubiquitous van der Waals (vdW) interaction, which for convenience is defined by us as the combination of size repulsion with dispersion attraction, including small induction contributions, is almost exclusively depending on the electronic polarizability of the interacting partners [18]. As previously, also in this study this aspect has represented an important guide line in planning and performing experiments under the same conditions for systems having similar vdW behavior, including that of interest and some reference cases. The applied methodology has been crucial to discover similarities and to isolate the role of the interaction components adding to vdW and providing further stabilization effects. Therefore, the use of experiments, carried out under specific conditions and combined to proper theoretical approaches [9], allowed us to underline in the investigated systems the nature of the interaction, with a detailed evaluation of its strength and of other specific features.

In the present paper, we focused our attention mostly on the water-CH_4 complex, for which are present in literature several theoretical [19–23] and few experimental [22, 24] studies, and on the H_2S-CH_4 system [20, 22]. This investigation represents an extension of previous studies on water-noble gas (Ng) [25], water-H_2 [26, 27] and hydrogen sulfide-Ng [28], hydrogen sulfide-H_2 systems [27]. As successfully applied in the past [9], our detailed study was performed by combining high-resolution scattering experiments, conducted with the molecular beam technique, with ab initio calculations made at the CCSD(T) level of theory, underlining the stereo-selectivity of the CT component, which emerges here in the perturbative limit and exhibits an exponential decreasing with the intermolecular distance [9].

Particular attention has been added to Ng-CH_4 systems, since taken as references in the present investigation, for which the results of extensive experimental and theoretical studies are available in literature [29–35]. Moreover, rotational spectra of CH_4-H_2S complex and deuterated isotopologues have been measured in this work, providing additional information and support to the discussion of the scattering and ab-initio data.

In the next section a brief description of the experimental techniques is reported, while the parameterization of the interaction potential together with the scattering and spectroscopic data analysis are described in section 3, where also a phenomenological comparison with reference systems is illustrated. The theoretical method and the results of the ab

initio calculations, concerning basic features of the interaction, crucial to rationalize the experimental findings, are discussed in section 4.

2. EXPERIMENTAL OVERVIEW AND DATA ANALYSIS

Molecular beam scattering experiments

Molecular Beam (MB) scattering experiments, performed in the thermal energy range, provide an excellent tool to investigate systems that present weak interactions as basic features driving the collisions. Detailed information about the absolute scale of the intermolecular interaction potential in two body systems can be obtained by measuring scattering cross sections and observing oscillating patterns due to quantum mechanical interference effects. In fact, they can be considered finger prints showing how the fragments interact during the formation of the collision complex. To reach these results, it is crucial to use an experimental apparatus operating under high angular and velocity resolution conditions [36]. The objective of the present study has been the measurement of the total (elastic plus inelastic) integral cross section $Q(v)$ as a function of the selected MB velocity v.

High resolution MB scattering experiments, performed under the same conditions on the system of interest and on properly chosen reference cases, allow observation and comparison of quantum interference's which are strictly related to similarities and to differences in the strength of the interaction driving the colliding partners.

In the present investigation, the quantum interference, called "glory effect", appears as an oscillating pattern in the velocity dependence of the measured integral cross section $Q(v)$. Therefore, the analysis of the experimental observations represent an excellent tool to define both the basic features of the interaction, in weakly bound systems including the possible role of an extra stabilization due to perturbative charge transfer (CT) effects.

The apparatus used has been extensively described elsewhere [36, 37]. Briefly, the setup is composed by a set of differentially pumped vacuum chambers where the MB is produced by a gas expansion from a nozzle source, maintained at a constant temperature. For the present experiments, it has been fixed at $\simeq$ 500 K in order to obtain rotationally hot molecules, to avoid the formation of clusters and to reduce the quenching of the measured glory amplitude [38], due to the interaction anisotropy [39]. Under the used conditions of temperature

and pressure (less than 10 mbar), the MB is generated with near effusive or moderately supersonic character. MB, collimated by two skimmers and a defining slit, is analyzed in velocity by a mechanical selector made by six slotted disks. Projectile molecules (water and hydrogen sulfide), flying at the selected MB velocity v, collide with the stationary target gas confined in the scattering chamber, and those not deflected by collisions are finally detected by a quadrupole mass spectrometer, which is coupled with an ion counting electronics. In addition, the scattering chamber has been maintained at 90 K to take advantage of the better resolution in the collision velocity, and has been filled with the gas target at $\simeq 10^{-3} - 10^{-4}$ mbar.

The fundamental quantity measured at each selected velocity v is the MB attenuation I/I_o: I represents the MB intensity attenuated by the collisions with the target in the scattering chamber and I_o the full MB intensity. From the I/I_o ratio measurement it is possible to determine the integral cross section $Q(v)$ through the Lambert-Beer law:

$$Q(v) = -\frac{1}{NL} \log \frac{I}{I_0} \ , \tag{1}$$

where N is the target gas density and L the effective path length of the scattering region [36]. The $Q(v)$ data measured as a function of v, are often plotted as $Q(v)v^{2/5}$ to emphasize the resolved oscillatory pattern due to the "glory" quantum interference structure. As we will discuss more in detail below such data provide detailed information on the absolute scale of the intermolecular interaction, both in the potential well and at long-range [40]. For the experiments with water beams, we have used D_2O instead of H_2O to take advantage of a smaller background signal at the detector. The present scattering cross sections of the isotopologue systems containing H_2O and D_2O, and the associated intermolecular intereactions, are expected to differ negligibly [26].

The measured $Q(v)$ are plotted in Figures 1 and 2. In Figure 1, the water-CH_4 cross sections are compared with those of O_2-CH_4, previously measured with the same apparatus under the same conditions (i.e. using as target CH_4 in the scattering chamber at 90 K) [41, 42], since O_2 exhibits an average electronic polarizability α similar to that of water (see Table 1). In the same Figure 2, present results for H_2S-CH_4 are also reported to show the dependence of the absolute $Q(v)$ values on the system. Further phenomenological information has been provided by the comparison (given in Figure 2) of the present scattering data with those previously measured by scattering a CH_4 MB by Ar and Xe targets. Indeed, Ar and Xe

atoms, having electronic polarizability similar to that of water and hydrogen sulfide (see Table 1), respectively, can be exploited to mimic the isotropic van der Waals behavior of fast rotating water and hydrogen sulfide molecules.

Rotational spectroscopy experiments

The rotational spectra of CH_4-H_2S and its isotopomers were recorded with the home-built Pulsed Nozzle Fourier Transform Microwave Spectrometer [43]. 1-2 % of CH_4 and H_2S were seeded into argon and the mixture was expanded from a back pressure of 0.5 atm to undergo supersonic expansion. At the pulsed nozzle, under the ambient conditions, due to three body collisions, the complex of CH_4 and H_2S was formed. This sample was polarized using a microwave pulse of duration 1.5 μs. 1000 shots of gas pulses were averaged to get a reasonable signal to noise ratio. The signals were checked for the component dependence by running the experiments in the absence of CH_4 and H_2S and the signals did not appear in the absence of either. To rule out any probability of the signal being dependent on the carrier gas, Ar, the signals were again recorded with He as the carrier gas. All the signal could be observed by using helium as a carrier gas, at a higher back pressure (1.2 atm). HDS/D_2S signals were observed by passing H_2S through HDO/D_2O. For this H_2S was passed through several bubblers placed sequentially which were filled with D_2O. The identity of the D_2S signals were confirmed by passing H_2S through a mixture of 50 % H_2O/D_2O, which diminished the CH_4-D_2S signals significantly because of the relative higher concentration of HDS in the expansion. The relative increase in HDS concentration was confirmed by monitoring the well known Ar-HDS and Ar-D_2S signals [44]. The samples e.g. Ar (99.999 %), CH4 (99.9 %) and H_2S (99.5 %) were obtained from Bhuruka Gases Ltd and were used without any further purification. D_2O (99.95 atom % D) was obtained from Sigma-Aldrich.

3. DATA ANALYSIS

Collision cross sections

Measured $Q(v)$ have been analyzed in order to extract the information on the strength of the intermolecular interaction potential V in a wide distance range. The model chosen to

represent the dependence of V on the intermolecular distance r, corresponds to the Improved Lennard Jones (ILJ) function [40]:

$$V(r) = \varepsilon \left[\frac{m}{n(r) - m} \left(\frac{r_m}{r} \right)^{n(r)} - \frac{n(r)}{n(r) - m} \left(\frac{r_m}{r} \right)^{m} \right] \quad (2)$$

The parameter ϵ represents the depth of the potential well, r_m is the equilibrium distance and n(r) is defined as:

$$n(r) = \beta + 4(\frac{r}{r_m})^2 \quad (3)$$

where β is a parameter related to the hardness of the colliding species and determines the shape of the potential well. β has been fixed to 9, the typical value for weak neutral-neutral bonded systems (also used in other experiments [25, 27]), while m is equal to 6 [40]. It is relevant to note that the ILJ formulation provides a long range attraction constant equal to $\varepsilon\, {r_m}^6$, whose value asymptotically reproduces the available ab initio dispersion coefficients [45]. A generalization of the ILJ model that includes an angular dependence of the interaction energy has been presented and validated elsewhere [30, 46, 47]. The scattering cross sections have been calculated from the assumed V with the semiclassical method in the center-of-mass (CM) framework (see Figure 3) and afterwards convoluted in the laboratory frame for a direct comparison with the measured $Q(v)$ [36]. Only the values of r_m and ϵ have been modified in order to obtain the fit of data. The main purpose has been the proper rationalization of the absolute value of $\bar{Q}(v)$, which depends on the long range attraction, and of the glory extrema position, related to the depth and position of the potential well [40]. This is sufficient to extract information on the absolute scale of V. It must be also emphasized that the reproduction of the glory amplitude, by using in the calculations a simple radial potential, is possible only for systems with low interaction anisotropy and involving fast rotating partners [25, 28, 38, 39]. Therefore the obtained parameters provide a measure of the average binding energy and equilibrium distance for the studied systems.

The final values ϵ and r_m, that characterize the ILJ, are reported in Table 1, where are also shown for comparison also the values predicted by the correlation formulas, exploiting the polarizability α_0 of the species and including the induction effect due to the permanent dipole of the water and H_2S [18]. The obtained interaction of water-CH_4 is in the right scale

of previous estimates coupling ab-initio data with information from experimental second virial coefficients [23, 48].

In both D_2O-CH_4 and H_2S-CH_4 systems, the observed glory structure (see Figure 2) is well described in frequency by the results of the simulations, so that the position of the maxima and the minima is well reproduced in both systems, but it is a well evident quenching in the amplitude oscillating pattern, especially in the water complex. The observed damping has been attributed to the pronounced anisotropy of the interaction [11]. According to the above observations and considering that the average $Q(v)$ values are practically coincident (within the experimental error) for D_2O, O_2, and Ar-CH_4 systems, the present findings [40] confirm that the long range attraction is the same in all the three cases and of vdW type. However, there is a evident shift at higher velocity of about 25% of the maxima and minima extrema in the water case, as better emphasized by the calculated CM cross sections plotted in Figure 3. In addition, while the O_2-CH_4 and Ar-CH_4 systems show a good agreement between the experimental and the predicted values (see Table 1), D_2O-CH_4 presents a value of the depth of the well about 5 meV larger than the predicted one. Both the findings suggest the occurrence of a further strongly stereo specific intermolecular bond stabilization adding to vdW. This extra stabilization should be attributed to the occurrence of the average CT effects. A different behavior in the absolute scale of the integral cross section $Q(v)$ can be emphasized by comparing the experimental data for D_2O-CH_4 and H_2S-CH_4 systems (see Figure 2). Moreover, the direct comparison of H_2S-CH_4 complex, done with Xe-CH_4 [29] (the same absolute scale of $Q(v)$) (see Figure 2), confirms the vdW nature of the long range attraction. Such comparison shows again a partial quenching of the "glory" amplitude in H_2S-CH_4, especially observable at higher v, accompanied by a less evident glory extrema shift (see Figure 3). This evidence suggests the occurrence of a less efficient stabilization due to CT. This findings is also corroborated by the smaller difference between experimental and predicted values of the potential parameters (see Table 1), respect to the water-CH_4 system.

Microwave spectrum

The first transition of the H_2S–CH_4 complex was observed at 5365.827 MHz and total of 10 transitions were observed [49]. The transition frequencies are given in Table 2 and

the fitted constants in Table 3. The 10 transitions observed were assigned to three different progressions and each progression could be fitted independently to a linear top. Fitting of the lines in Progression I of the parent compound gave the rotational constant, B = 2683.097(1) MHz and the distortion constant, D_J = 0.09390(7) MHz. Progression II and III lines on fitting gave slightly smaller rotational constants, B=2638.2575 MHz and 2593.05 MHz respectively. However, the fitting led to negative values for the distortion constants as, D_J = -0.5209 MHz for Progression II and D_J = -0.0089 MHz for progression III. This negative distortion constant implies rotational-vibrational coupling present in the molecule. These two progressions arise from some excited internal rotor/torsional states. The rotational constants for the isotopomers CH_4–HDS and CH_4–D_2S were also predicted from the rotational constants of CH_4–H_2S and are reported elsewhere [49]. Some information can be obtained form the analysis of the three progressions in the spectrum. The main conclusion is that in the complex the monomers undergo internal rotation. The fact that the transitions could be fitted to linear top indicates that the two monomers can be considered as two interacting spheres. If it is so, then the monomers can undergo free rotation with respect to the other. Therefore the microwave spectrum suggest that the intermolecular interaction for the CH_4–H_2S is relatively isotropic. Considering CH_4 and H_2S as two spherical units, the intermolecular separation can be calculated from the ground state rotational constant, B. This comes out to be 4.13 Åfor CH_4–H_2S. Similar values have been obtained for the other isotopomers. This number is consistent with that obtained from the analysis ofi the measured collision cross section (4.23 Å, see Table 1). The spectroscopy experiment has been performed with cold molecules and therefore, even if the complex is relatively floppy, a restricted configuration space has been explored. On the other hand, the scattering data provide a consistently slightly larger distance since hot molecules have been used and the experiments probed the whole configurations of the complex.

The spectroscopic results on CH_4–H_2S complex can be compared with similar literature data on CH_4–H_2O [24]. In this case the analysis of the microwave spectra performed with a simple internal-rotation models suggested that the CH_4–H_2O water interaction is more anisotropic than that of Ar–H_2O. For CH_4–H_2O complex, K = 1 lines could be assigned whereas for the CH_4–H_2S complex K = 1 lines could not be assigned yet. This finding is consistent with the scattering results. Moreover, the fit of the microwave spectrum provided an equilibrium constant of 3.67 Å, for the CH_4–D_2O isotopomer which agrees nicely with

the value of 3.77 Å determined from the present scattering experiments on CH_4–D_2O (see Table 1). Note the similar difference in the intermolecular separation determined from spectroscopic and scattering experiments for both these complexes.

THE AB-INITIO INTERMOLECULAR INTERACTION ENERGY

The main purpose of the theoretical calculations have been: to define the most stable configurations of the systems, to rationalize the differences in water-CH_4 and H_2S-CH_4, with the Ar-CH_4 and Xe-CH_4 cases, respectively, and to confirm the vdW nature of the intermolecular bond in Ar, Xe-CH_4 systems. Many ab-initio calculations of water methane PES have been done in the past and has been reviewed in a recent paper of Bowman and coworkers [50]. Much less information is available for the H_2S-CH_4 case [22].

Computational details

The calculations of the energetic and structure of the CH_4-H_2X (with X=O,S) complexes have been carried out at the coupled cluster level of theory [51, 52] with single, double (CCSD) and perturbative triple excitations (CCSD(T)) using augmented correlation-consistent polarized basis sets of increasing size (aug-cc-pVXZ, X= T, Q, 5) [53, 54]. The program MOLPRO has been used throughout [55]. Weak intermolecular interactions, as the present ones, leave the geometry of the monomers essentially unaffected. During the geometry optimization of the aggregate, the two interacting molecules have thus been kept rigid at their free equilibrium structure [56], being V of the order of ten meV (few kJ/mol) as maximum. The H-S distance was fixed at 1.33 Å [27] and the H-S-H angle is 92.2 degrees, while the H-O distance is 0.9716 Å and H-O-H angle is 104.69 degrees [27]. For the CH_4 molecule the H-C distance and the H-C-H angle are, respectively, 1.086 Å [34] and 109.471 degrees. BSSE was not corrected in the geometry optimiation.

The analyzed structures of the complexes have been specified by five coordinates (Figure 4): one distance r and four angles α, θ, ϕ, and β. r is the module of the position vector, $\vec{r}$, and represents the distance of the center of mass (cm) of H_2X molecule from the carbon atom of the methane (origin of the coordinate system). α is the angle between the C_2 symmetry axis of H_2X and $\vec{r}$ (α=0 and α=180 correspond, respectively, to H_2X pointing the

methane molecule with the X atom or the two hydrogens), while θ, the angle between $\vec{r}$ and the C_3 methane symmetry axis (with θ=0, 55, 180 representing H_2X pointing, respectively, the vertex, the edge and face of CH_4), indicates the revolution around the methane. ϕ corresponds to the dihedral angle between the H_2X plane and the σ_v plane of CH_4, containing the C_3 symmetry axis (ϕ=0, the H_2X hydrogen atoms lying on the σ_v methane plane and ϕ=90 the hydrogen atoms are perpendicular to it and on the same side). Finally, β describes the rotation angle of H_2X around its C_2 symmetry axis.

Four different minimum energy walks of the total Potential Energy Surface (PES), that can be distinguished during the revolution of H_2X around CH_4 (see Figure 6), have been studied. Maintaining fixed ϕ=0, three of such walks are identified as α=0, α=180 and $\alpha \simeq$130 and correspond to H_2X approaching the methane pointing, respectively, with the X atom, and having both hydrogen atoms and with only an hydrogen atom (specifically α=126.5 for the water and 133.5 for H_2S) lying on the σ_v CH_4 plane. The fourth path is called "Perp", and the revolution is done by imposing ϕ=90.

We performed, finally, a full optimization of the intermolecular variables (the distance r and the four angles α, θ, ϕ, and β) at the CCSD(T)/aug-cc-pVTZ level of theory for the most relevant local minima points (see below), followed by single point (SP) calculations, over the optimized geometries, by varying the basis set (aug-cc-pVQZ), and using the aug-cc-pV5Z for some specific arrangements (see tables 4,5).

Results

For both the complexes, passing from the aug-cc-pVTZ to the aug-cc-pVQZ, the convergence seems to be fast achieved for the corrected interaction energies $E_{int,BSSE}$ respect to the uncorrected E_{int} values. In fact, the difference is$\simeq$ 4-5 meV for the uncorrected energies, and $\simeq$ 1-2 meV for the corrected ones. For the H_2O–CH_4 complex, the binding energy of the global and secondary minima, without BSSE correction, agree very well (3.0 %) with the CCSD(T)/CBS result of Ref. [23].

Some energy profiles for the CH_4-H_2O and CH_4-H_2S systems, corrected for BSSE [57], are reported, in the upper and lower panels panels of Figure 6, respectively, as function of the revolution angle θ (from 0 to 360 in steps of 10). The panels of the Figure 7 show the behavior of the optimized equilibrium distance (r_e) values, in the four different arrangements,

by maintaining fixed the angular variables during the revolution (see caption for details).

The results of the calculations, plotted in Figure 6, clearly indicate that for some specific configurations the water shows a stronger interaction than the H_2S (the energy range may lower up to -40 meV against ca. -30 meV). In particular, the various cuts with CH_4 are slightly different from each other, suggesting that in specific geometries the attractive component at intermediate and short distance is more efficient for water respect to the hydrogen sulfide. The first relevant point, focusing on the cuts at θ=0, is that for the water system the most stable configuration is when the oxygen points the hydrogen of the methane (α=0, ϕ=0), while for H_2S when is perpendicular to the σ_v plane (α=0, ϕ=90). This difference may be sought to the different role of the stabilizing components. However, the most stable geometry shows the same configuration for both the systems, and occurs for θ=180, when the hydrogen points the methane face ($\alpha \simeq$130 and ϕ=0). In the case of water such configuration is stabilized very much respect to the other geometries, suggesting a probable pronounced role of the CT, but for H_2S it results almost isoenergetic to that with the hydrogen pointing the tetrahedral face (α=180 and ϕ=0).

As indicated above, in the global minimum geometry the H_2X points the tetrahedral face of the methane with an hydrogen atom (θ=180), suggesting, in the case of water, the formation of a more pronounced "hydrogen bond" structure [22]. For the water system, these two minima configurations, i.e. the analyzed secondary minimum (θ=0, α=0, ϕ=0) and the global minimum, are quite similar both in geometry and in energy to the ab-initio values reported in literature [23, 48, 50, 58].

Passing to $\theta \simeq$60, i.e. when H_2X points the edge of the methane, the energies become more negative, introducing a stronger interaction between the fragments, respect to θ=0, and an increasing "hydrogen bond" character is shown in both systems. From these energy effects and analyzing the PES's cuts reported in Figure 6 for both CH_4-H_2X systems, it is noticeable that the energy scale is different, indicating that the various components of the interaction change their specific role, leading to a more pronounced anisotropy in the water complex. Moreover, for a proper rationalization of the experimental findings, it is necessary to evaluate the different strength of the interaction, and also is relevant to compare the interaction anisotropy occurring in CH_4-H_2X respect to that in the reference CH_4-Ng systems, for which has been observed a limited glory quenching.

We characterized the most relevant local minima, and the results of the optimized struc-

tures, as the uncorrected/corrected interaction energies values and equilibrium distances r_e, obtained at the CCSD(T)/aug-cc-pVTZ level of theory for such basic arrangements, are reported in Tables 4,5 for a proper comparison.

The anisotropy and stereo specificity of the interaction

In this section, the main focus is on the interaction anisotropy, in order to justify its different role in the systems of interest and in the reference ones, and to rationalize the observation of a pronounced quenching of the glory amplitude, especially in water-methane.
In Table VI are reported, for a direct comparison, the intermolecular features of the CH_4-Ng (with Ng=Ar,Xe) systems for θ= 0,55,180 (respectively, vertex, edge and face geometries) arrangements, calculated at the CCSD(T) level of theory with different basis sets (aug-cc-pVXZ for Ar and aug-cc-pVXZ-PP [59] for Xe, with X=T,Q,5). In the same Table are also reported, for a comparison, the results predicted with the "atom-bond" model [30], useful to describe the anisotropic vdW PESs. It is eye-catching that, passing from the aug-cc-pVTZ to the aug-cc-pV5Z basis set, the agreement with the experiment improves and the ab-initio 5Z $r_{e'}$ parameters, which represent the minimum position of the energy curves corrected for the BSSE, get closer to the predicted values, while the predicted energies are mostly found between the uncorrected E_{int} and corrected $E_{int,BSSE}$ energies. This comparison suggests that it is necessary to use high and accurate basis sets to reach the predicted values, which are in the proper scale of the experimental determinations [29].

For the CH_4-H_2X systems, the comparison of calculations with the phenomenological potential, obtained from the analysis of the present experimental data (see previous section and Table VI), is more complicated since the absolute scale of the probed interaction is determined by the average over several configurations of the full configuration space. Previous estimates of the PES and the effective average potentials have been present in refs [23, 48, 50] and the overall agreement of the latter with the present experimental value is acceptable. One should also consider that present ab-initio CCSD(T) calculations suggest that calculated values converge towards the experimental ones as the size of the basis set is increased. Moreover, as indicated above, the V_{vdW} component for the CH_4-H_2X (with X=O,S) complexes, averaged over the H_2X orientations, must be close to that of CH_4-Ar and CH_4-Xe systems, because of the comparable polarizability (see Table 1) of water and

hydrogen sulfide molecules with Ar and Xe atoms, respectively. Therefore, the comparison of the cuts of the PES, evaluated at the same level of theory, should provide additional information on nature and on different anisotropy of the interaction.

In Figure 7 is compared the behavior of the ab initio (CCSD(T)/aug-cc-pVTZ) revolution paths (optimizing the intermolecular distance) of Ng atoms around the methane molecule with that of CH_4-H_2X, obtained following the minimum energy path (MEP), particular, considered to represent a measure to the anisotropy in CH_4-H_2X cases. The revolution reported was made from θ= 0 to θ= 180 in step of 5 degrees for the Ng systems to better emphasize the edge geometries. As described previously and as affirming in Figure 7, the behavior of the interaction in the CH_4-Xe/H_2S systems is similar and explainable mostly with a different role of stereo specific and anisotropic components, that lead to a further stabilization. A most significant role is mainly expected when H_2S points the methane edge and face with an hydrogen atom ($\theta \simeq$ 60, 180). This geometry has been interpreted as the S-H—C hydrogen bonded earlier [22] On the other hand, analyzing the CH_4-Ar/H_2O systems, it is very clear that the two methane partners interact very differently. In fact, with the water molecule, the energy oscillation is more evident and, as noticeable from the experiments, the CT can play, in addition to the induction, a more pronounced role compared to the case of H_2S. Since such component must be stereo selective, it strongly affects the interaction anisotropy, lowering very much the energies in specific geometries, as the vertex, edge and face of the methane respect to the Ar partner. All these suggestions, obtained from a direct analysis of the PES's cuts, fully justify the experimental observation of a pronounced glory amplitude quenching observable in both CH_4-H_2X systems and more evident in CH_4-water case.

The above results and discussion have been recently substantiated [60] by an extensive analysis of the Charge Displacement (CD) function [9] carried out for all the above studied systems and including also the CH_4-Ng (Ng=Ar,Xe) complexes. This analysis shaded light onto, and also quantified, the electron density rearrangement, due to both polarization and charge transfer, taking place upon the formation of the intermolecular complexes. In particular, the analysis of the CH_4-Ng (Ng=Ar,Xe) complexes suggested that here the interaction arises from the balance of size repulsion with dispersion attraction (V_{vdW}). Since electrostatic contributions are absent, this analysis evidenced that also induction and CT components are negligible for the CH_4-Ng complexes. This is confirmed by the behavior of

the CD function, which exhibits only a small electron polarization effect on the Ng atom, due to presence of the permanent electric octupole moment on CH_4.

In addition, as expected, the strenght of the electric dipole induced on Ng has been found to decrease as r^{-5} (more details are given in ref. [60]). The same analysis performed on CH_4-H_2X complexes suggests that electrostatic, induction and CT components increase in importance with respect to CH_4-Ng systems, requiring a detailed description and a more complex modeling of the intermolecular interaction. The first difference with respect to the CH_4-Ng systems is related to the permanent electric dipole moment of the H_2X molecules which induces a significant distortion of the electronic distribution of methane, with an evident polarization in all the basic geometries of the aggregates, and an effect of induction on the involved total intermolecular potential V.

Moreover, it has been found (see ref. [60] for details) that the contribution of CT to the interaction between H_2X and methane is not-negligible and follows a similar pattern in the two H_2X-CH_4 systems investigated, even if with different magnitudes. Water acts as a more efficient donor and electron acceptor with respect to H_2S, manifesting already in this perturbative limit its more pronounced acid and basic character [27]. This is in a agreement with the experimental observations of a different glory quenching and shifting and with the modifications in the microwave spectra for the two intermolecular complexes. Since the role of CT is so evident and important, a monitoring of its falloff with the distance has been performed and resulted consistently in an exponential decreasing behavior [9, 60].

Finally, a more detailed analysis has been carried out for a specific configuration (*vertex*) of the CH_4-H_2O system along the $\alpha = 0$ revolution walk (see Fig. 4). Herein, the various interaction components have been properly modelled according to semiempirical and empirical formulas, and the predicted energies have been compared with the ab-initio CCSD(T) and DFT-SAPT results. This effort represents an important probe of proposed potential models which is suitable for extension to systems at increasing complexity.

Accordingly, the total interaction potential V has been defined as a balance of few effective components: size repulsion, combined with dispersion attraction, represented as a sum of atom–bond contributions [30], each of one defined by an ILJ function; the induction associated to the permament dipole-molecular bond contributions, each one proportional to $\mu_w^2\ \alpha_{C-H}\ r^{-6}$, where μ_w is the water dipole and α_{C-H} the polarizability of the C-H bond; the stabilization due to CT, that has been considered as proportional to the amount of electron

transfer, evaluated at the isodensity point of the CD curves between the two fragments (see ref. [60]); the electrostatic term, arising from the Coulomb interaction between the charges on the molecular frames responsible of the permanent methane octupole moment and the permanent water dipole. The latter interaction component has been assumed to decay proportionally to r^{-5} at large r. The proportionality between CT and stabilization energy and their exponential decreasing with r has been fully demonstrated by us and by many other authors for both the weak intermolecular hydrogen and halogen bondings [9, 61–63].

All the contributions have been added to obtain V. The proposed potential model provides a reasonable reproduction of ab-initio interaction energy cut (CCSD(T)/aug-cc-pVQZ corrected for the BSSE [57]), both in the well depth value (model: -29.8 meV, ab-initio: -28.0 meV) and in the equilibrium distance position (model: 3.82 Å, ab-initio: 3.80 Å). Note that the difference between the model and the ab-initio (not corrected for the BSSE: -30.5 meV) is of the order of the BSSE [57] correction ($\simeq$ 2 meV). The DFT-SAPT calculations, with the same aug-cc-pVQZ basis set, provided results coincident with CCSD(T).

A benefit of this approach is the possibility to estimate the relative role of the main interaction components in a wide intermolecular distance range. For the examined case, the major relative role at the equilibrium distance has been found for the dispersion component which accounted for $\simeq$ 55 % of the total stabilising energy (see also ref. [23]). Induction, electrostatic and CT terms played a minor, but still significant, role since contributing to 8, 23 and 14 % of the total interaction, respectively. Such results can be compared with those from the DFT-SAPT decomposition, as shown in Table VII.

In particular, it is evident that the results from the present approach and those from the DFT-SAPT method are consistent for the total energy, while some of the partitioned components appear to be method dependent. Specifically, while the dispersion and induction attractions obtained by the DFT-SAPT decomposition (46 % and 9 % respectively of the global stabilisation energy, respectively) are in a substantial agreement with those of the present approach (see above), the major differences (see Table VII) appear in the values of the size repulsion (exchange-repulsion in SAPT) and of the electrostatic term. As discussed above, in our approach the electrostatic component has been estimated by using the semiempirical formula based on the permanent dipole and permanent octupole moment of the interacting molecules. This formula is appropriate for intermolecular distances larger than the molecular dimensions. At shorter distances, it can lead to an underestimation of

electrostatic energy. In addition, size repulsion and dispersion attraction components have been obtained by extending to anisotropic systems the ILJ potential model adopted in the fitting of the experimental data. In the SAPT decomposition, the dispersion attraction is provided by the second order correction. The exchange repulsion and the electrostatic term are both obtained by the first order perturbation theory even at short distances, where substantial overlap effects occur. It is a challenging task and it can be not accurate. However, it is important to note that the sum of size repulsion (exchange-repulsion) with electrostatic terms is very similar for ours and SAPT methodologies (14.6 meV and 17.3 meV, respectively) suggesting a possible compensation of the effects.

The CT energy obtained by us from the charge displacement analysis is independent from any definition of electrostatic or size repulsion energies. Indeed, it has been demonstrated that such an analysis is valid and accurate for many systems where the electrostatic term is null [9]. Furthermore, standard SAPT calculations cannot provide direct information on CT energy, which is normally absorbed into other terms (essentially in induction attraction) [63]. It is noteworthy to note that the CT energy we have determined is fully consistent with that one can estimate using a recently proposed procedure based on a modification of SAPT methodology [9, 63].

CONCLUSIONS

New experiments involving water and hydrogen sulfide molecular beams scattered by methane target have been performed to measure the total (elastic plus inelastic) integral cross section as a function of the beam velocity. Complementary information have been obtained by rotational spectra, recorded for the hydrogen sulfide-methane complex, with a pulsed nozzle Fourier transform microwave spectrometer. The objective of this investigation has been the characterization of range, strength and anisotropy of the intermolecular potential in water, hydrogen sulfide-methane, which are important complexes, especially for their technological applications (clathrates hydrates). Measured data have been compared with those previously obtained by using the same experimental methodology for some reference systems, containing methane and the other partner, chosen according to similar value of the electronic polarizability (the fundamental physical property defining size repulsion, dispersion and induction attraction) of water and hydrogen sulfide, respectively.

Specifically, water-CH_4 has been compared with Ar,O_2-CH_4, while H_2S-CH_4 with Xe-CH_4. The comparison suggested that, while the long range attraction in water-CH_4 is practically the same as in Ar,O_2-CH_4, at intermediate and short distances the intermolecular potential exhibits a different strength and a more pronounced interaction anisotropy respect to the reference systems.

A similar situation occurs for H_2S-CH_4 respect to Xe-CH_4, although in the intermediate region the difference is less pronounced compared to the previous cases. Clearly, though the intermolecular potentials in both cases show anisotropy, it is more marked in the case of CH_4-H_2O compared to that for CH_4-H_2S.

Extensive ab initio calculations have been performed to rationalize all the experimental findings. The obtained results have been exploited also to perform important tests of the theoretical methods, usually applied to evaluate weak intermolecular potentials. Moreover, such results represent an important starting point to understand the relative role of the an important interaction component, as the charge transfer, whose stereo specificity can affect substantially the topology of the full potential energy surface and, as a consequence, the control of the molecular dynamics, both in gas and condensed phases.

Aknowledgments

This work was supported by the Italian Ministero dellIstruzione, della Ricerca e dellUniversit (PRIN 2010-2011, Grant No. 2010ERFKXL-002).

* Electronic address: david.cappelletti@unipg.it

[1] G. C. Maitland, M. Rigby, E. B. Smith, and W. A. Wakeham, *Intermolecular forces: their origin and determination* (Claredon Press, Oxford, 1987).

[2] E. Arunan, G. R. Desiraju, R. A. Klein, J. Sadlej, S. Scheiner, I. Alkorta, D. C. Clary, R. H. Crabtree, J. J. Dannenberg, P. Hobza, et al., Pure and App. Chem. **83**, 1637 (2011).

[3] A. C. Legon, Angew. Chemie Int. Ed. **38**, 2686 (1999).

[4] A. Falenty, T. C. Hansen, and W. F. Kuhs, Nature **516**, 231 (2014).

[5] E. D. Sloan, Nature **426**, 353 (2003).

[6] G. R. Desiraju, Acc. Chem. Res. **29**, 441 (1996).

[7] U. Koch and P. Popelier, J. Phys. Chem. **99**, 9747 (1995).

[8] V. Aquilanti, E. Cornicchi, M. Moix Teixidor, N. Saendig, F. Pirani, and D. Cappelletti, Angew. Chemie Int. Ed. **44**, 2356 (2005).

[9] D. Cappelletti, E. , L. Belpassi, F. Tarantelli, and F. Pirani, Acc. Chem. Res. **45**, 1571 (2012).

[10] E. Arunan and D. Mani, Farad. Discus. **177**, 51 (2015).

[11] D. Cappelletti, A. Bartocci, F. Grandinetti, S. Falcinelli, L. Belpassi, F. Tarantelli, and F. Pirani, Chem. Eur. J. **21**, 6234 (2015).

[12] A. Bartocci, L. Belpassi, D. Cappelletti, S. Falcinelli, F. Grandinetti, F. Tarantelli, and F. Pirani, J. Chem. Phys. **142**, 184304 (2015).

[13] M.-L. Dubernet, F. Daniel, A. Grosjean, A. Faure, P. Valiron, M. Wernli, L. Wiesenfeld, C. Rist, J. Noga, and J. Tennyson, Astron. Astrophys. **460**, 323 (2006).

[14] N. Crockett, E. Bergin, J. Neill, J. H. Black, G. Blake, and M. Kleshcheva, Astrophys. J. **781**, 114 (2014).

[15] S. Falcinelli, F. Pirani, and F. Vecchiocattivi, Atmosph. **6**, 299 (2015).

[16] H. Lee, J.-W. Lee, J. Park, Y.-T. Seo, H. Zeng, I. L. Moudrakovski, C. I. Ratcliffe, and J. A. Ripmeester, Nature **434**, 743 (2005).

[17] E. D. Sloan Jr and C. Koh, *Clathrate hydrates of natural gases* (CRC press, 2007).

[18] R. Cambi, D. Cappelletti, G. Liuti, and F. Pirani, J. Chem. Phys. **95**, 1852 (1991).

[19] S. R. Ungemach and H. F. Schaefer III, J. Am. Chem. Soc. **96**, 7898 (1974).

[20] D. E. Woon, P. Zeng, and D. R. Beck, J. Chem. Phys. **93**, 7808 (1990).

[21] J. B. Martins, J. R. Politi, E. Garcia, A. F. Vilela, and R. Gargano, J. Phys. Chem. A **113**, 14818 (2009).

[22] B. Raghavendra and E. Arunan, Chem. Phys. Lett. **467**, 37 (2008).

[23] O. Akin-Ojo and K. Szalewicz, J. Chem. Phys. **123**, 134311 (2005).

[24] R. Suenram, G. Fraser, F. Lovas, and Y. Kawashima, J. Chem. Phys. **101**, 7230 (1994).

[25] L. F. Roncaratti, L. Belpassi, D. Cappelletti, F. Pirani, and F. Tarantelli, J. Phys. Chem. A **113**, 15223 (2009).

[26] L. Belpassi, M. L. Reca, F. Tarantelli, L. F. Roncaratti, F. Pirani, D. Cappelletti, A. Faure, and Y. Scribano, J. Am. Chem. Soc. **132**, 13046 (2010).

[27] A. Bartocci, D. Cappelletti, F. Pirani, F. Tarantelli, and L. Belpassi, J. Phys. Chem. A **118**, 6440 (2014).

[28] V. Aquilanti, D. Cappelletti, F. Pirani, and L. F. Roncaratti, Int. J. Mass Spectrom. **280**, 72 (2009).

[29] G. Liuti, F. Pirani, U. Buck, and B. Schmidt, Chem. Phys. **126**, 1 (1988).

[30] F. Pirani, M. Alberti, A. Castro, M. M. Teixidor, and D. Cappelletti, Chem. Phys. Lett. **394**, 37 (2004).

[31] F. Pirani, D. Cappelletti, and G. Liuti, Chem. Phys. Lett. **350**, 286 (2001).

[32] Y. Liu and W. Jäger, J. Chemical Phys. **120**, 9047 (2004).

[33] Q. Wen and W. Jäger, J. Chem. Phys. **124**, 014301 (2006).

[34] T. Heijman, T. Korona, R. Moszynski, P. Wormer, and A. Vanderavoird, J. Chem. Phys. **107**, 902 (1997).

[35] W. A. Alexander and D. Troya, J. Phys. Chem. A **110**, 10834 (2006).

[36] D. Cappelletti, M. Bartolomei, F. Pirani, and V. Aquilanti, J. Phys. Chem. A **106**, 10764 (2002).

[37] F. Pirani, M. Bartolomei, V. Aquilanti, M. Scotoni, M. Vescovi, D. Ascenzi, D. Bassi, and D. Cappelletti, J. Chem. Phys. **119**, 265 (2003).

[38] E. Luzzatti, F. Pirani, and F. Vecchiocattivi, Mol. Phys. **34**, 1279 (1977).

[39] V. Aquilanti, D. Ascenzi, D. Cappelletti, M. de Castro, and F. Pirani, J. Chem. Phys. **109**, 3898 (1998).

[40] F. Pirani, S. Brizi, L. F. Roncaratti, P. Casavecchia, D. Cappelletti, and F. Vecchiocattivi, Phys. Chem. Chem. Phys. pp. 5489–5503 (2008).

[41] G. Liuti and F. Pirani, J. Chem. Phys. **87**, 5266 (1987).

[42] V. Aquilanti, F. Pirani and D. Cappelletti, J. Chem. Soc. Faraday Trans. **89**, 1467 (1993).

[43] E. Arunan, A. Tiwari, P. K. Mandal, and P. C. Mathias, Curr. Sci. **82**, 533 (2002).

[44] H. Gutowsky, T. Emilsson, and E. Arunan, J. Chem. Phys. **106**, 5309 (1997).

[45] T. N. Olney, N. Cann, G. Cooper, and C. Brion, Chem. Phys. **223**, 59 (1997).

[46] M. Albertì, A. Castro, A. Laganà, M. Moix, F. Pirani, D. Cappelletti, and G. Liuti, J. Phys. Chem. A **109**, 2906 (2005).

[47] M. Alberti, A. Aguilar, J. M. Lucas, F. Pirani, D. Cappelletti, C. Coletti, and N. Re, J. Phys. Chem. A **110**, 9002 (2006).

[48] Z. Cao, J. W. Tester, and B. L. Trout, J. Chem. Phys. **115**, 2550 (2001).

[49] P. Aiswaryalakshm, Ph.D. thesis, Indian Institute of Science, Bangalore, India (2013).

[50] C. Qu, R. Conte, P. L. Houston, and J. M. Bowman, Phys. Chem. Chem. Phys. **17**, 8172 (2015).

[51] K. Raghavachari, G. W. Trucks, J. A. Pople, and M. Head-Gordon, Chem. Phys. Lett. **157**, 479 (1989).

[52] C. Hampel, K. A. Peterson, and H.-J. Werner, Chem. Phys. Lett. **190**, 1 (1992).

[53] J. Thom H. Dunning, J. Chem. Phys. **90**, 1007 (1989).

[54] D. E. Woon and J. Thom H. Dunning, J. Chem. Phys. **98**, 1358 (1993).

[55] H. Werner, P. Knowles, R. Lindh, F. Manby, and M. Schütz, MOLPRO version 2012.1 a package of ab initio programs 2012 see http://www. molpro. net **1**, 1 (2012).

[56] G. Herzberg, *Electronic Spectra and Electronic Structure of Polyatomic Molecules* (Van Nostrand, New York, 1966).

[57] S. Boys and F. Bernardi, Mol. Phys. **19**, 553 (1970).

[58] K. L. Copeland and G. S. Tschumper, J. Chem. Theo. Comp. **8**, 1646 (2012).

[59] K. A. Peterson, D. Figgen, E. Goll, H. Stoll, and M. Dolg, J. Chem. Phys. **119**, 11113 (2003).

[60] A. Bartocci, F. Frati, L. Roncaratti, D. Cappelletti, F. Tarantelli, L. Belpassi, and F. Pirani, Molecular Physics, accepted for publication (2015).

[61] R. Z. Khaliullin, A. T. Bell and M. Head-Gordon, Chem. Eur. J. **15**, 851 (2009).

[62] C. Wang, D. Danovich, Y. Mo and S. Shaik, J. Chem. Theory Comput. **10**, 3726 (2014).

[63] A. J. Stone and A. J. Misquitta, Chem. Phys. Lett. **473**, 201 (2009).

[64] A. J. Misquitta, R. Podeszwa, B. Jezioski and K. Szalewicz, J. Chem. Phys. **123**, 214103 (2005).

TABLE I: Well depth ε (meV) and equilibrium distance r_m (Å) for the D_2O-CH_4, H_2S-CH_4, O_2-CH_4 and Xe-CH_4 systems. The predicted results, obtained with the correlation formulas [18], are reported as references[18, 25]. The average polarizabilities α (Å^3) of the various X partners in the X-CH_4 system are also reported [45].

	experimental		predicted		
system X-CH_4	ε	r_m	ε	r_m	α(X)
D_2O-CH_4	17.50	3.77	13.18	3.87	1.47
O_2-CH_4	13.90	3.89	12.99	3.92	1.60
Ar-CH_4	14.04	3.88	12.87	3.95	1.64
H_2S-CH_4	18.50	4.23	17.36	4.16	3.78
Xe-CH_4	18.50	4.31	19.16	4.19	4.04

TABLE II: Experimentally observed rotational transitions (MHz) of CH_4–H_2S complex.

	progression I	progression II	progression III
$J_{1\leftarrow 0}$	5365.827		5186.105a
$J_{2\leftarrow 1}$	10729.387	10583.405	10372.485
$J_{3\leftarrow 2}$	16088.437	15870.149	15559.236
$J_{4\leftarrow 3}$	21440.744	21244.323	

TABLE III: Fitted Rotational Constant (B), Distortion Constant (D_J) (MHz) for CH_4–H_2S complex

	Progression I	Progression II	Progression III
B	2683.097(1)	2638.2575	2593.05(1)
D_J	0.09390(7)	-0.5209	-0.0089(7)

TABLE IV: Optimized intermolecular variables (interaction energies E_{int}, equilibrium distances r_e and four angles α, θ, ϕ, and β) of the CH_4-H_2O complexes at the CCSD(T)/aug-cc-pVTZ level of theory for the different revolution paths minima (See Text). The results of single point calculations (SP), done over the full optimized geometries by using different basis set (aug-cc-pVXZ, with X=Q,5), are shown.

basis	r (Å)	θ	α	ϕ	β	E_{int} (meV)	$E_{int,BSSE}$ (meV)
TZ	3.74	0.0	0.0	0.0	180.0	-34.0	-26.5
QZ						-30.6	-27.8
5Z						-29.21	-28.23
TZ	3.80	0.0	0.0	90.0	180.0	-28.8	-19.6
QZ						-23.83	-20.70
5Z							
TZ	3.70	53.4	123.1	0.0	180.0	-40.3	-30.2
QZ						-35.1	-31.5
5Z							
TZ	3.46	180.00	126.5	0.0	180.0	-51.3	-39.2
QZ						-45.8	-41.1
5Z				0.0		-43.51	-41.64
TZ	3.48	189.8	180.0	0.0	180.0	-34.8	-27.7
QZ						-32.5	-29.4
5Z						-30.93	-29.84

TABLE V: Optimized intermolecular variables (interaction energies E_{int}, equilibrium distances r_e and four angles α, θ, ϕ, and β) of the CH_4-H_2S complexes at the CCSD(T)/aug-cc-pVTZ level of theory for the different revolution paths minima (See Text). The results of single point calculations (SP), done over the full optimized geometries by using different basis set (aug-cc-pVXZ, with X=Q,5), are shown.

basis	r (Å)	θ	α	ϕ	β	E_{int} (meV)	$E_{int,BSSE}$ (meV)
TZ	4.27	0.0	0.0	0.0	180.0	-22.7	-14.6
QZ						-17.7	-15.5
5Z						-17.00	-15.71
TZ	4.30	0.0	0.0	90.0	180.0	-27.2	-18.6
QZ						-22.9	-19.7
5Z							
TZ	4.23	55.5	132.7	0.0	180.0	-31.3	-21.9
QZ						-26.8	-23.1
5Z							
TZ	4.02	180.00	127.6	0.0	180.0	-40.7	-30.4
QZ						-36.1	-31.9
5Z							
TZ	3.88	190.1	180.0	0.0	180.0	-39.0	-29.9
QZ						-35.0	-31.7
5Z							

TABLE VI: Comparison, between the features of three relevant cuts of the PES's: the binding energies corrected $E_{int,BSSE}$ (meV) and not E_{int} (meV) for the BSSE, and the equilibrium distance ($r_{e'}$ (Å)) for the CH_4-Ng (with Ng=Ar,Xe) complexes evaluated at the CCSD(T) level with different basis sets (aug-cc-pVXZ, with Z=T,Q,5) and the values predicted by the "atom bond" model [30] (Pred.). The $r_{e'}$ values correspond to the minimum position of the energy curves corrected for the BSSE.

System	Source	θ=0			θ=55			θ=180		
		$r_{e'}$	E_{int}	$E_{int,BSSE}$	$r_{e'}$	E_{int}	$E_{int,BSSE}$	$r_{e'}$	E_{int}	$E_{int,BSSE}$
CH_4-Ar	TZ	4.30	-15.82	-9.55	4.00	-17.45	-12.12	3.70	-21.86	-14.88
	QZ	4.20	-13.28	-10.36	3.90	-16.01	-13.41	3.70	-19.59	-16.46
	5Z	4.20	-12.70	-10.64	3.90	-15.75	-13.87	3.70	-19.18	-17.00
	Pred.	4.18	-10.50		3.85	-15.70		3.77	-17.20	
CH_4-Xe	TZ	4.60	-19.88	-13.31	4.30	-22.12	-16.25	4.10	-26.66	-19.65
	QZ	4.6	-16.63	-14.46	4.20	-20.32	-17.93	4.00	-24.59	-21.75
	5Z	4.60	-15.86	-14.78	4.20	-19.71	-18.55	4.00	-23.85	-22.53
	Pred.	4.47	-15.01		4.14	-22.56		4.05	-24.11	

TABLE VII: The interaction components, in meV, are indicated according to the formulation of our model (see text) and to the DFT-SAPT decomposition scheme (see [64])

present		DFT-SAPT/aug-cc-pvQZ	
Size Repulsion	28.1	Exchange Repulsion ($E^{(1)}_{Exch.}$)	47.9
Dispersion	-31.9	Dispersion ($E^{(2)}_{Disp.}$+$E^{(2)}_{Exch-Disp.}$)	-34.7
Induction	-4.64	Induction ($E^{(2)}_{Ind.}$+$E^{(2)}_{Exch-Ind.}$)	-7.30
Electrostatic	-13.5	Electrostatic $E^{(1)}_{elst.}$	-30.6
CT	-7.7	-	
-		δ_{HF}	-3.30
Total energy	-29.8	Total energy	-28.0

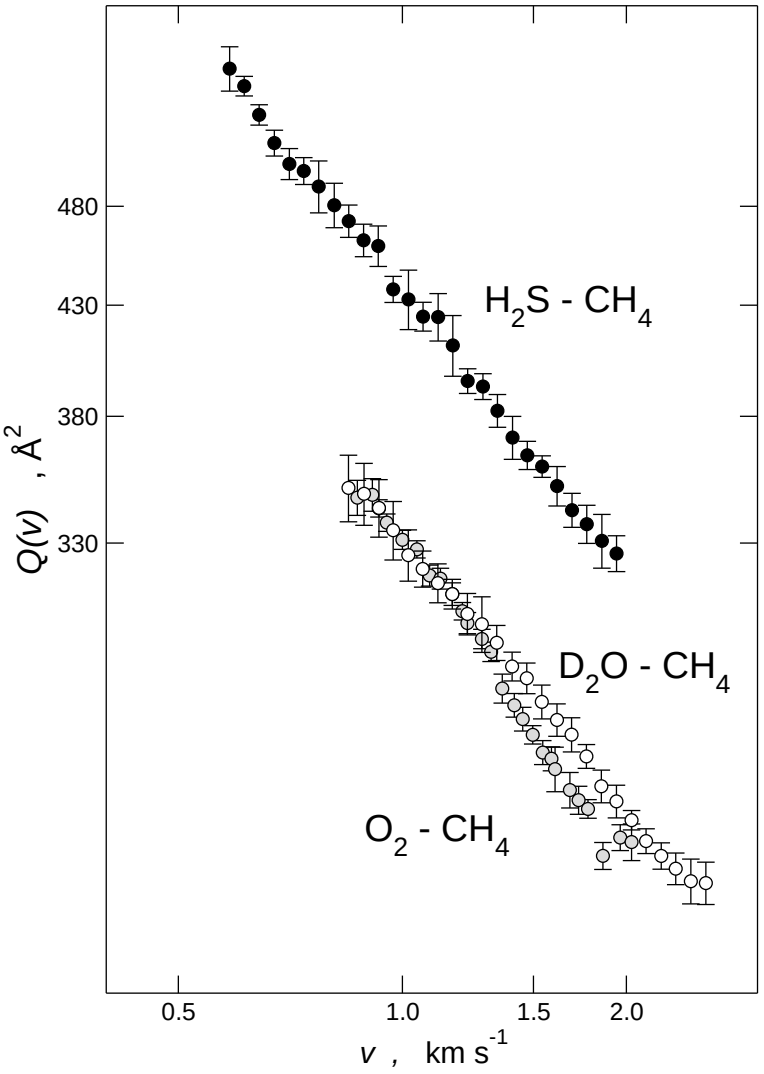

FIG. 1: Integral cross sections $Q(v)$, plotted as a function of the selected MB velocity v, for the H_2S-CH_4, D_2O-CH_4, and O_2-CH_4 systems.

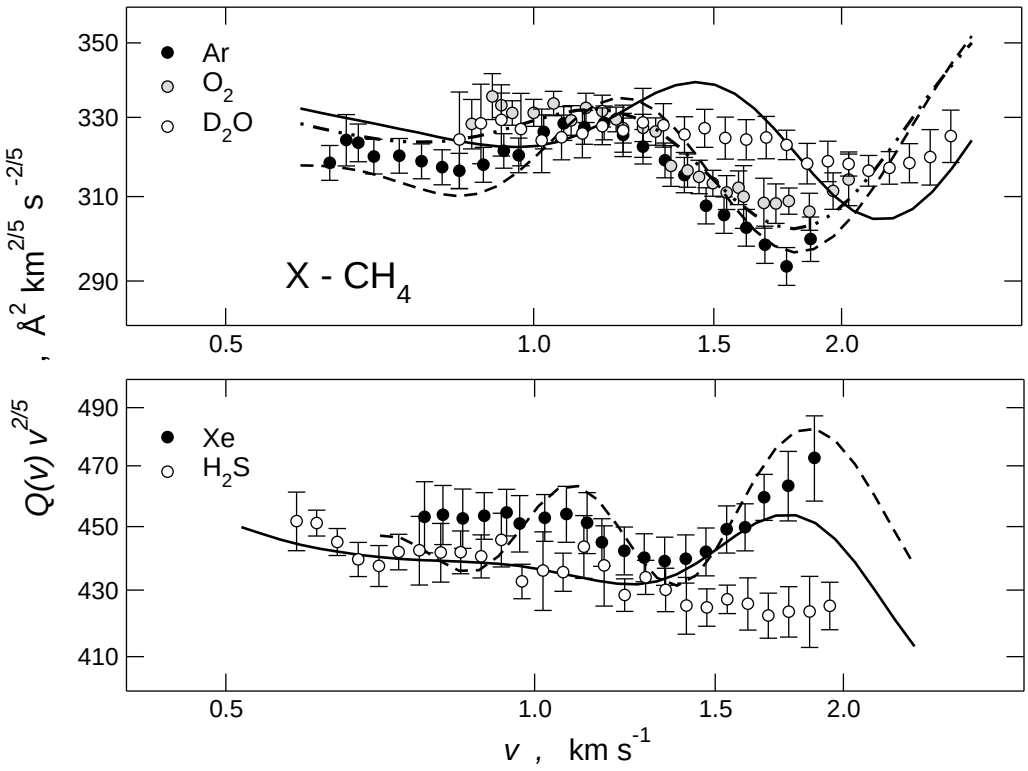

FIG. 2: Integral cross sections $Q(v)$ for the X-CH_4 systems. Data are plotted as $Q(v)\,v^{2/5}$ [40] to emphasize the glory patterns. Upper panel: comparison between Ar-CH_4, O_2-CH_4 and D_2O-CH_4. Lower panel: comparison between Xe-CH_4 and H_2S-CH_4.

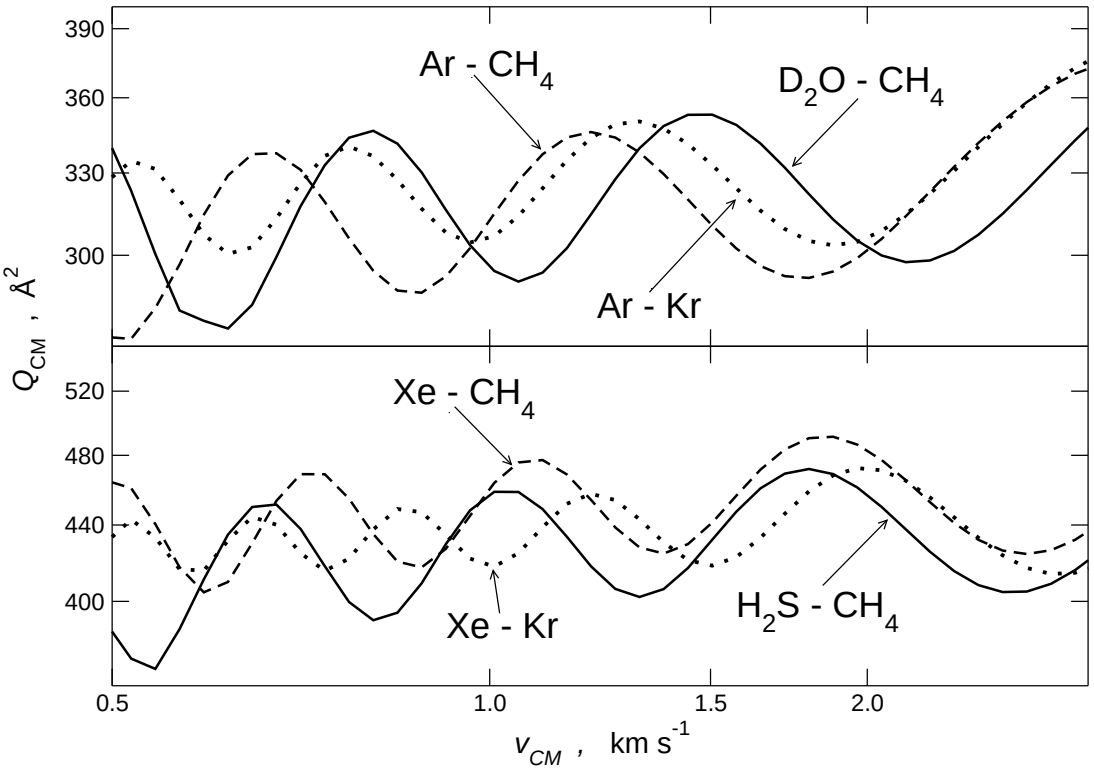

FIG. 3: Comparison of the integral cross section calculated in the frame of the CM to well emphasize and underline the glory shift between the systems. Upper panel: comparison between Ar-CH_4, Ar-Kr and D_2O-CH_4. Lower panel: comparison between Xe-CH_4, Xe-Kr and H_2S-CH_4.

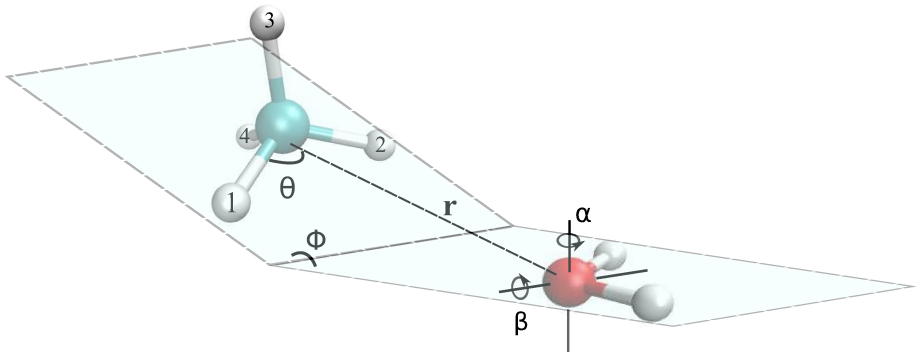

FIG. 4: Sketch of the coordinate system adopted in the present work. All the atoms are confined in the two planes except hydrogens 3 (above the plane) and 4 (below the plane). θ is the angle between $\mathbf{r}$ and the CH_1 bond.

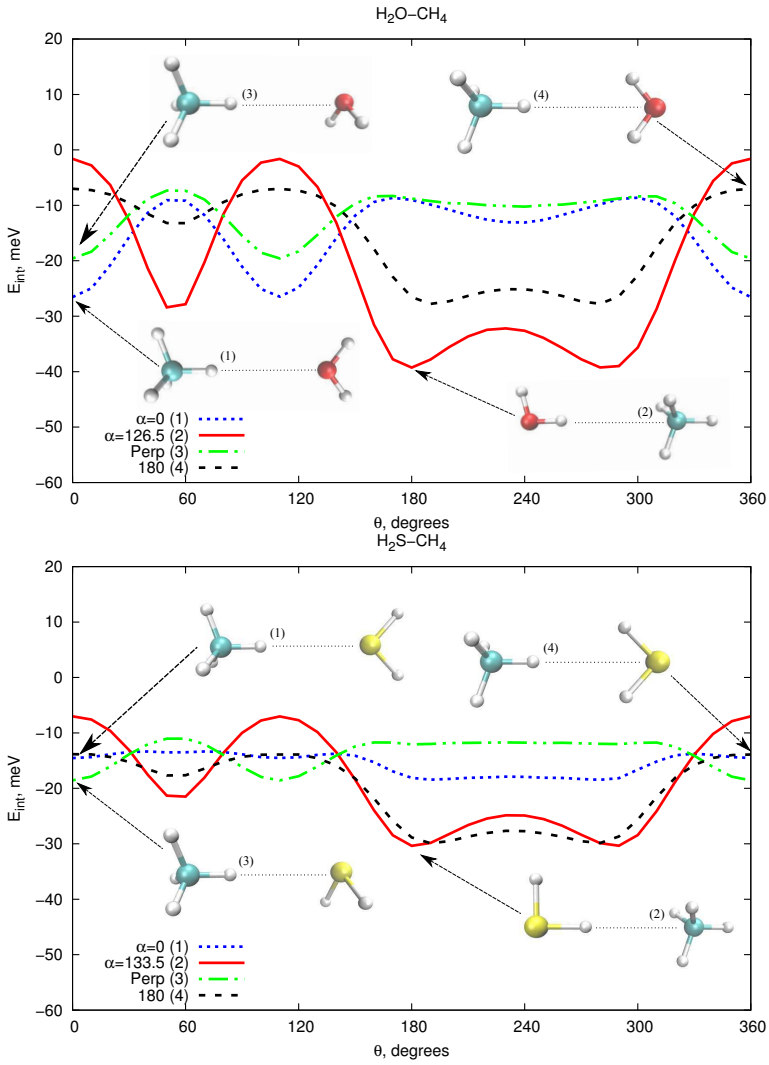

FIG. 5: CCSD(T)/aug-cc-pVTZ interaction energies E_{int} as a function of the orientation angle θ in the α=0, α=180, α=133, and Perp arrangements (see text) for the CH_4-H_2O (upper panel) and CH_4-H_2S (lower panel) system. The values of E_{int} are corrected for BSSE.

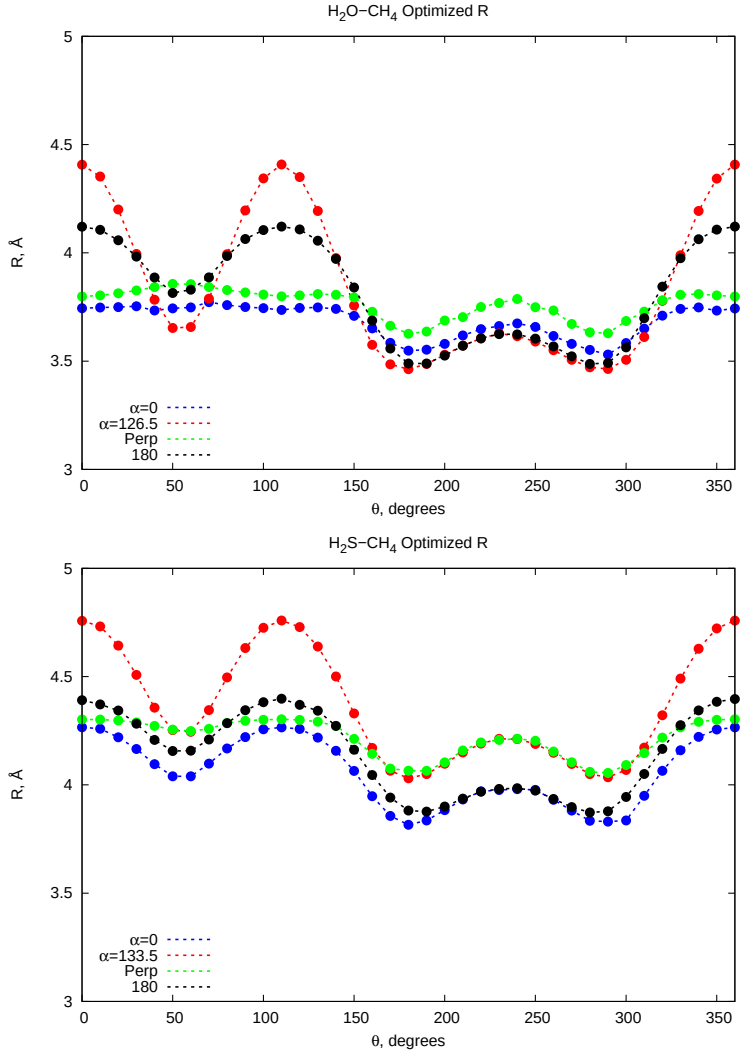

FIG. 6: Behavior of the optimized equilibrium distance r_e (Å) at the CCSD(T)/aug-cc-pVTZ level of theory as a function of the orientation angle θ in the α=0, α=180, α=133, and Perp arrangements (see text) for the CH_4-H_2O (upper panel) and CH_4-H_2S (lower panel) system.

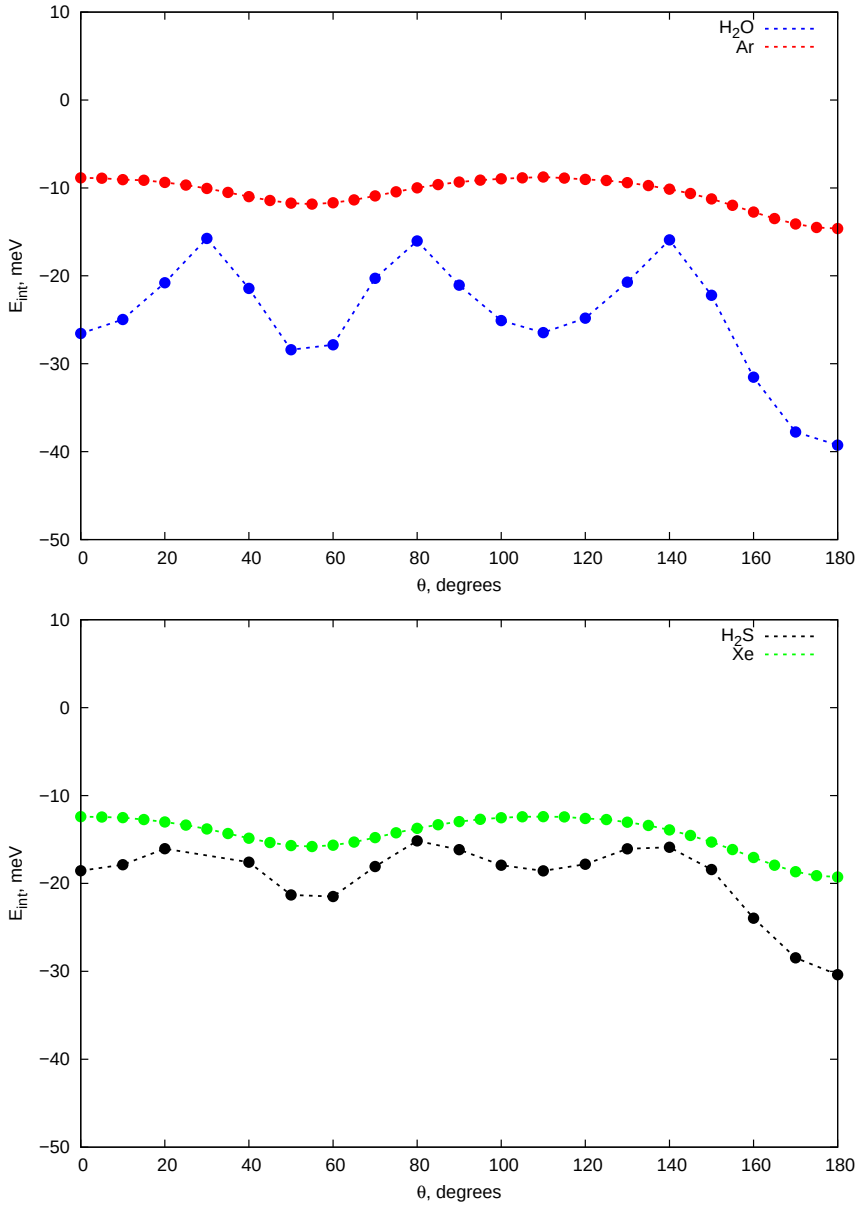

FIG. 7: Comparison between the CCSD(T)/aug-cc-pVTZ interaction energies E_{int} as a function of the orientation angle θ for the CH_4-Ng and the minimum energy path (MEP), obtained by taking the lower cuts in Figure 6, for CH_4-H_2X systems. Since they have a comparable polarizability (see Table I), in the upper panel are compared CH_4-Ar/H_2O and in the lower panel CH_4-Xe/H_2S. The values of E_{int} are corrected for BSSE.